International Journal of Geo-Information

MDPI

Article

Mapping the Invisible: Integrating Nighttime Light and Social Sensing to Explore Hidden Cross-Border Economies

Xiaofang Zhai [1], Fan Zhang [1], Zhifeng Xiao [2,*], Haoyang Xu [1] and Weiqi Yan [3]

[1] School of Urban and Environmental Sciences, Hubei Normal University, Huangshi 435002, China; zhaixf@hbnu.edu.cn (X.Z.); zhfan@stu.hbnu.edu.cn (F.Z.); xhaoyang0828@163.com (H.X.)
[2] State Key Laboratory of Information Engineering in Surveying, Mapping and Remote Sensing (LIESMARS), Wuhan University, Wuhan 430079, China
[3] Computer and Information Sciences, Auckland University of Technology, Auckland 1010, New Zealand; weiqi.yan@aut.ac.nz
* Correspondence: xzf@whu.edu.cn

Abstract

Against the backdrop of the continuing spread of cross-border telecommunications fraud and the scarcity of conventional data, this study examines how publicly accessible multi-source data can be used to monitor and characterize the spatiotemporal evolution of known or suspected fraud compounds under data-scarce conditions. Focusing on eight representative and manually delineated fraud compounds in Myanmar's border regions, it develops a three-dimensional "space–time–representation" framework that integrates 2017–2025 VIIRS nighttime lights (NTL), Sentinel-1/2-derived built-up area (BUA) expansion, and Baidu Index time series as a proxy for Chinese-language public attention. Dynamic time warping (DTW) is used to examine temporal alignment between NTL dynamics and public attention, while spatial autocorrelation and exploratory grouping based on DTW dissimilarity are applied to characterize spatial clustering and heterogeneous temporal patterns. The results show that BUA expansion and nighttime brightness are not uniformly coupled across compounds and years. After excluding partial-year 2025 observations, the complete-year 2017–2024 park–year analysis indicates weak aggregate associations between BUA and annual mean NTL, highlighting the need to interpret the two indicators as complementary but non-equivalent proxies. NTL changes do not necessarily evolve synchronously with changes in public attention, suggesting potential value for monitoring and prioritization rather than direct early-warning or verification of illicit activities. The global Moran's I of 0.2476 indicates significant spatial clustering of nighttime-light values within the defined compound–buffer analysis units. DTW alignment reveals stronger consistency between nighttime lights and Baidu Index attention in the Daxiang and Dingsheng compounds, whereas KK Park and Yatai City show weaker public-search responses relative to observed NTL dynamics. Exploratory grouping identifies three patterns of NTL–public attention correspondence, highlighting heterogeneous relationships between observed nighttime-light dynamics and external information visibility. The study demonstrates the complementarity of remote sensing and social sensing data under data scarcity and proposes a replicable approach for remote monitoring, typological characterization, and evidence-informed governance prioritization of known or suspected fraud compounds. The proposed approach should be interpreted as a screening and analytical framework that provides directional evidence rather than as direct verification of illicit activity or compound-specific operational status.

Keywords: cross-border telecommunications fraud; nighttime lights (NTL) remote sensing; built-up area (BUA); social sensing; fraud compound monitoring

Check for updates

Academic Editors: Wei Jiang and Wolfgang Kainz

Received: 13 July 2026
Revised: 2 October 2026
Accepted: 10 October 2026
Published: 15 October 2026

Copyright: © 2026 by the authors. Published by MDPI on behalf of the International Society for Photogrammetry and Remote Sensing. Licensee MDPI, Basel, Switzerland. This article is an open access article distributed under the terms and conditions of the Creative Commons Attribution (CC BY) license.

1. Introduction

Against the backdrop of rapid global digital infrastructure expansion and fragmented geopolitical governance, cross-border telecommunications fraud has evolved into a "non-traditional security–economic" hybrid risk that combines regional embeddedness with transnational mobility [1]. The borderlands of Southeast Asia, shaped by regulatory gaps, armed fragmentation, and the coupling of capital–violence networks, have emerged as spatial hubs associated with such criminal activities [2]. In particular, northern Myanmar's so-called economic zones," "technology parks," or "free trade areas" operate under legitimizing narratives, while engaging in telecommunications fraud through illegal detention, coercion, and highly organized operations, forming spatially concentrated fraud compounds characterized by concealment, governance complexity, and limited accessibility for field investigation [3]. In this study, the cross-border spaces commonly referred to as 'scam parks' or 'fraud camps' are operationally defined as fraud compounds/enclaves, referring to the spatially bounded sites selected for analysis based on publicly reported information and manual delineation from satellite imagery. Due to the sensitivity barriers surrounding internal law enforcement data, traditional site-based investigations and field data collection face high costs, risks, and ethical concerns. Consequently, research must shift toward openly accessible remote sensing and online search data to reconstruct and characterize the spatiotemporal evolution of known or suspected fraud compounds under conditions where field investigation and official data are limited.

Conceptually, these compounds can be situated within broader debates on sacrifice zones, NIMBY dynamics, and environmental justice communities. Although fraud compounds differ from conventional environmental sacrifice zones because their harms are associated with coercive digital labor, cross-border cyber-fraud, and restricted mobility rather than pollution or industrial land use, they similarly reflect how marginalized spaces can become sites where social, legal, and infrastructural vulnerabilities are concentrated. Previous studies on sacrifice zones emphasize the intersection of territorial marginalization, power relations, and the neglect of vulnerable communities, while research on geospatial planning and environmental justice highlights the need to connect spatial technologies with more inclusive governance responses [4,5]. This perspective helps frame fraud compounds not only as isolated illicit facilities but also as manifestations of digital socio-spatial injustice in borderland regions.

Nighttime light (NTL) remote sensing, due to its high sensitivity to electricity consumption and human activity, has become a key indicator for measuring spatial activity intensity. In recent years, it has been widely applied in fields such as urban expansion monitoring [6], disaster assessment [7], poverty identification [8] and the analysis of socioeconomic and human activity patterns in data-scarce regions [9]. Existing studies indicate that in data-scarce or monitoring-restricted regions, NTL data can provide valuable information on population activity, infrastructure development, and economic dynamics. This makes them particularly suitable for characterizing spatial activity changes and monitoring areas where direct observation is difficult, including conflict-affected or governance-constrained regions [10,11]. However, a single remote sensing approach remains limited in interpretive depth and cannot adequately reveal external information visibility, public attention dynamics, or social responses associated with spatial changes.

Meanwhile, social media search intensity has recently emerged as an important proxy indicator for quantifying public attention and the strength of social responses. User search behaviors are conceptualized as immediate reactions to external events, crises, or policy shifts and have been validated in domains such as disaster monitoring, epidemic diffusion analysis, and social risk perception, demonstrating strong temporal sensitivity and responsiveness [12,13]. However, in sensitive regions such as gray spaces, ad-

ministrative censorship and algorithmic filtering cause systemic information loss [14–16], while user self-censorship and silence induce expressive bias [17], undermining data representativeness and generalizability. Therefore, social media data are best treated as complementary evidence to remote sensing observations rather than as standalone indicators [18]. In this study, Baidu Index is therefore interpreted as a proxy for external Chinese-language information attention rather than a direct measurement of local activity or public perception in Myanmar.

Although both NTL and online search intensity hold promise for monitoring cyber-fraud enclaves, systematic empirical studies integrating these complementary data sources to characterize the spatiotemporal evolution of known or suspected fraud compounds remain limited [19]. Existing literature exhibits two main gaps: (1) the temporal granularity mismatch between monthly composite NTL data and high-frequency, real-time social media data has largely been addressed only at a technical calibration level, with limited methodological theorization [20]; (2) the interpretation of online attention data in data-scarce and governance-constrained regions remains challenging because information visibility may be affected by platform characteristics, media exposure, and uneven participation patterns. Therefore, social sensing indicators require contextual interpretation and integration with independent spatial observations [21].

Beyond cyber-fraud-specific studies, recent advances in spatial crime analysis have demonstrated the value of integrating spatiotemporal information, environmental characteristics, and computational approaches for understanding the geographic dynamics of illicit activities. Recent studies have explored spatiotemporal crime prediction and spatial optimization frameworks, examined the influence of urban environmental characteristics on crime patterns, and developed deep learning models for fine-scale crime analysis by capturing complex spatial–temporal dependencies [22–24]. However, these approaches generally rely on relatively complete crime records or dense urban sensing data, which are often unavailable in remote border regions and concealed illicit spaces. Accordingly, this study does not aim to predict crime occurrence but focuses on reconstructing and characterizing the observed spatiotemporal evolution of known or suspected fraud compounds using publicly accessible remote sensing and social sensing indicators.

This study takes eight representative and manually delineated fraud enclaves in northern Myanmar (Huanya Park, Dingsheng Park, KK Park, Jinxin Park, Daxiang Park, Baisheng Park, Yatai City Park, and Yulongwan Park) as case studies, addressing the challenges of field-based investigations in sensitive areas. It proposes and implements a three-dimensional data fusion framework of "space–time–representation", wherein Sentinel-1/2-derived built-up area represents physical expansion, nighttime lights (NTL) represent nighttime activity intensity, and the Baidu Index represents external information visibility and public attention. It systematically analyzes the spatiotemporal coupling features among physical expansion, activity intensity, and information visibility across multiple data sources, aiming to reconstruct the observed temporal trajectories and variation patterns of fraud compounds and provide methodological support for remote, multidimensional monitoring of cross-border gray economies.

The core challenge of this study lies in how, under the absence of on-site verification, to utilize the complementarity among nighttime lights, land expansion, and public attention indicators to reconstruct and characterize the observed spatiotemporal trajectories of fraud compounds and identify potential abnormal variations in multi-source indicators. To address this challenge, the study applies Dynamic Time Warping (DTW) to achieve asynchronous alignment between nighttime light and public attention sequences, employs spatial autocorrelation to examine spatial clustering and local deviations, and utilizes clustering methods to summarize similarity-based temporal patterns. It further explores tem-

poral variations and lead–lag relationships among multi-source indicators across different temporal stages and discusses the potential transferability of the framework to data-scarce regions such as Cambodia. Based on this empirical design, the study reconstructs the observed temporal trajectories of the compounds, reveals lead–lag structures and variation patterns between nighttime lights and public attention, and evaluates the potential applicability of the framework in data-scarce regions, providing methodological and empirical support for remote monitoring and comparative analysis of cyber-fraud compounds.

2. Materials and Methods

2.1. Study Area

The study area is located in the Myanmar border regions where the selected compounds are located, mainly along the Myanmar–Thailand border corridor in Kayin State and selected eastern border areas of Shan State (approximately 16.63–20.47° N, 98.47–99.90° E), as seen in Figure 1. Within this region, eight representative cross-border telecommunications fraud enclaves—Huanya Park, Dingsheng Park, KK Park, Jinxin Park, Daxiang Park, Baisheng Park, Yatai City Park, and Yulongwan Park—are selected for analysis. Some are located less than 2 km from an international border, with the nearest site approximately 1.3 km away based on Google Maps (web-based platform; accessed on 16 June 2025). The region is characterized by complex governance conditions, fragmented administrative control, and the coexistence of multiple armed actors, creating challenges for conventional field investigation and spatial monitoring [25]. To further characterize the selected compounds, Table 1 summarizes their coordinates and geographic settings, while Figure 2 presents Google satellite imagery and the manually delineated boundaries used for subsequent NTL and BUA extraction. Together, these materials provide the park-level spatial context necessary for interpreting the following remote-sensing analyses.

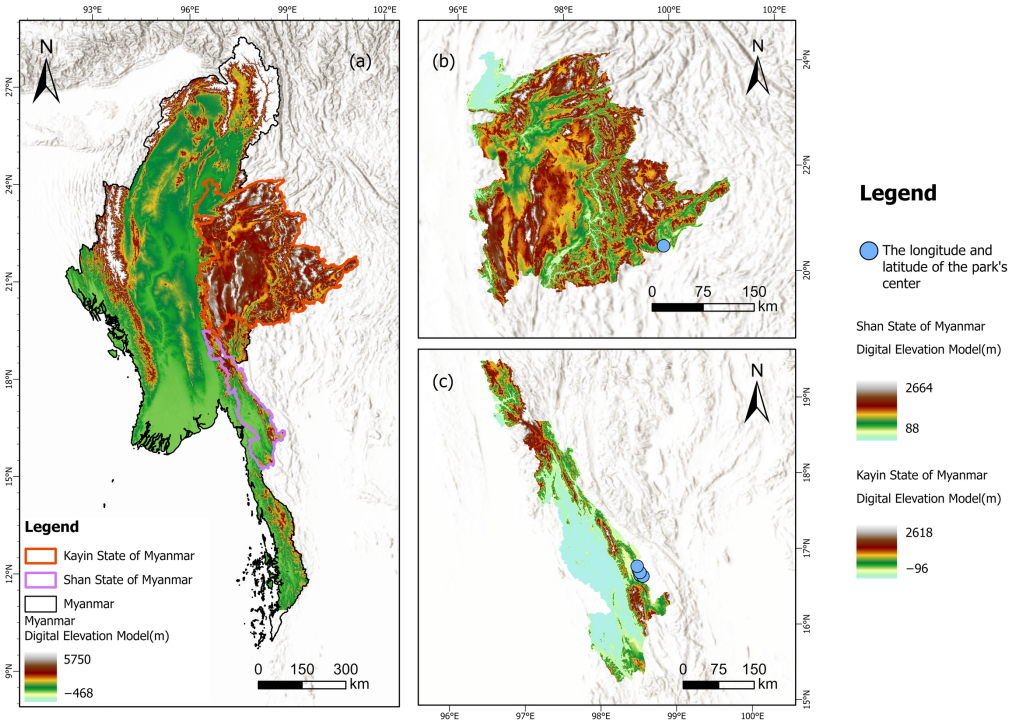


Figure 1. Spatial distribution of telecommunications fraud parks in selected Myanmar border regions (**a**–**c**). (**a**) Location of Kayin State and Shan State within Myanmar; (**b**) topographic setting of Shan State and park location; (**c**) topographic setting of Kayin State and park locations.



Figure 2. Google satellite imagery of the eight telecommunications fraud compounds. (**a**) Huanya Park; (**b**) Dingsheng Park; (**c**) KK Park; (**d**) Jinxin Park; (**e**) Daxiang Park; (**f**) Baisheng Park; (**g**) Yatai City Park; (**h**) Yulongwan Park. Geographic characteristics were interpreted from Google Earth imagery and manually delineated park boundaries. Satellite image cutouts were exported from Google Earth imagery.

Table 1. Geographic characteristics of the eight telecommunications fraud parks. Coordinates are expressed in WGS84 decimal degrees and refer to the approximate centroid or main built-up area of each park.

Park Name	Coordinates	Geographic Characteristics
Huanya Park	16.645675° N, 98.515339° E	Located near the China–Myanmar/Thailand–Myanmar borderland corridor; clustered with other parks in the Myawaddy border area.
Dingsheng Park	16.709154° N, 98.493630° E	Located in the borderland cluster, close to cross-border transport corridors and nearby fraud-park agglomerations.
KK Park	16.631998° N, 98.554395° E	Located near the Moei/Thaungyin River border zone, with evident built-up expansion in a peripheral border setting.

Table 1. *Cont.*

Park Name	Coordinates	Geographic Characteristics
Jinxin Park	20.466185° N, 99.901514° E	Located in an eastern Shan State border area, away from the main Myawaddy–Mae Sot cluster, and characterized by a relatively peripheral borderland setting.
Daxiang Park	16.698551° N 98.763576° E	Located on the eastern periphery of the Myawaddy–Mae Sot borderland corridor, surrounded by dispersed built-up areas and transport-accessible settlement land.
Baisheng Park	16.680132° N, 98.515773° E	Located within the Myawaddy-area park cluster, close to other suspected fraud-park sites.
Yatai City Park	16.826939° N 98.466185° E	Located north of the main Myawaddy-area cluster, close to the borderland river corridor and adjacent transport routes.
Yulongwan Park	16.763577° N, 98.477743° E	Located north of the main Myawaddy cluster, close to borderland transport and settlement corridors.

2.2. Data Collection

To construct a spatiotemporal monitoring and characterization framework for cyber-fraud enclaves, this study integrates multiple heterogeneous sources of publicly accessible data covering three dimensions: spatial activity intensity, physical development extent, and online public attention.

2.2.1. Nighttime Light Data

For spatial monitoring, one of the core data sources used in this study is VIIRS Nighttime Light (NTL) imagery from 2017 to 2025, provided by the U.S. National Oceanic and Atmospheric Administration (NOAA). Owing to its high sensitivity to nighttime surface radiance, it has been widely applied in urban expansion monitoring, conflict detection, and disaster assessment. As shown in Figure 3, the nighttime light time series indicates a continuous increase in overall brightness since 2017, with a sharp rise observed in early 2023, stabilization at a high level in early 2024, and notable declines in May and August, approaching baseline levels by early 2025. This brightness evolution temporally overlaps with selected publicly reported periods of concentrated disclosure of telecom fraud cases within China, cross-border law enforcement operations in the Wa region in 2024, and large-scale repatriation events in 2025, as shown in Figure 3. To facilitate clearer visual interpretation of nighttime-light dynamics, Figure 3 presents six representative compounds selected from the eight study sites. These six compounds have relatively larger spatial extents, making their temporal trajectories and spatial changes more visually distinguishable at the VIIRS spatial resolution. The remaining two smaller compounds are not displayed in this illustrative figure to maintain readability, but all eight compounds were included in the subsequent quantitative analyses.

Spatially, several parks near the border showed changes from low-radiance areas to higher-radiance clusters in the NTL imagery. Overall, nighttime light intensity serves as an indirect proxy for nighttime activity intensity and electricity-use-related surface radiance. Therefore, NTL changes are interpreted as screening signals for monitoring and prioritization rather than direct evidence of illicit activity or enforcement-related responses [26,27].

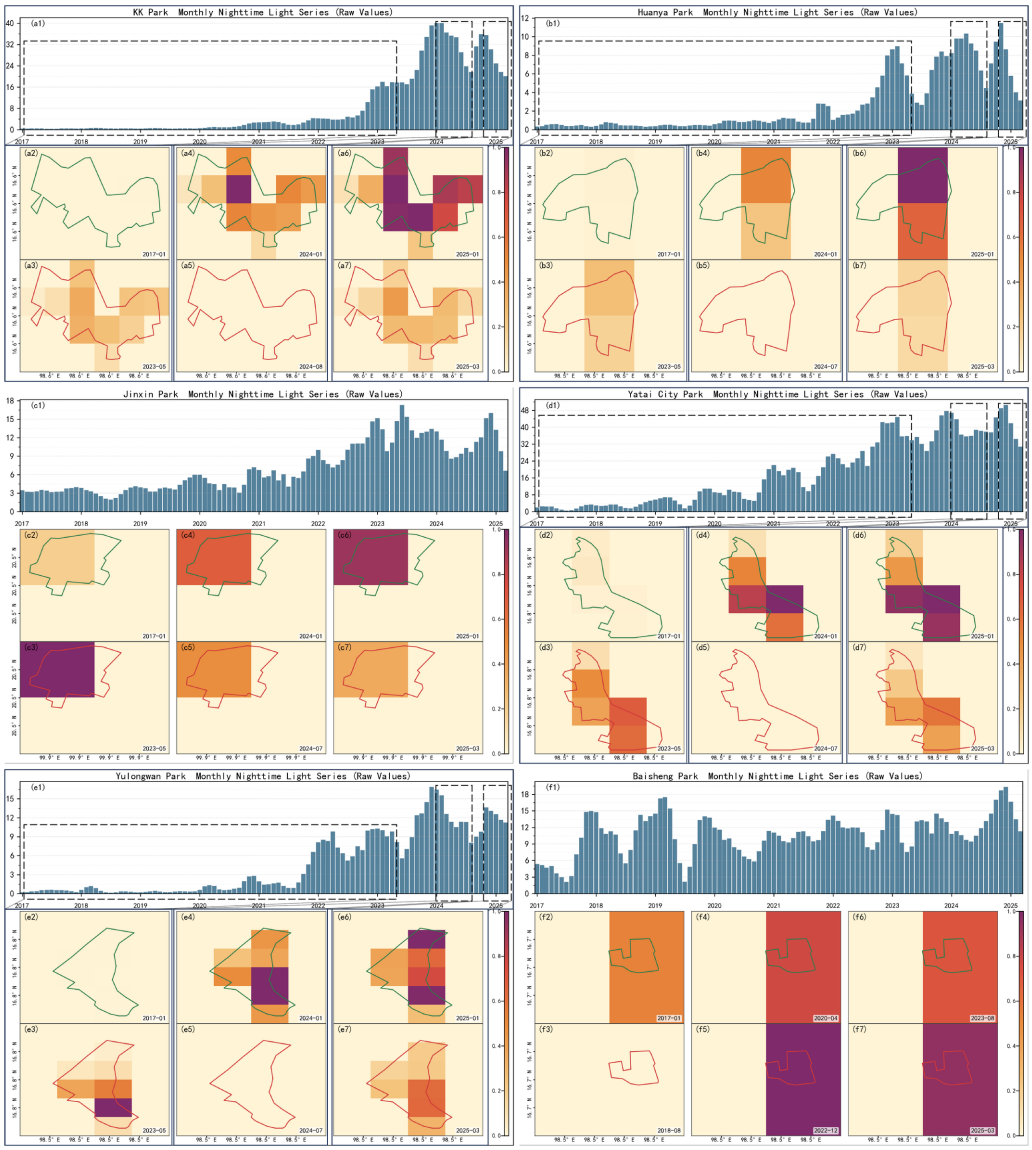


Figure 3. Representative nighttime-light dynamics and spatial snapshots for six larger selected compounds. Panels (**a1–a7**) show KK Park, panels (**b1–b7**) show Huanya Park, panels (**c1–c7**) show Jinxin Park, panels (**d1–d7**) show Yatai City Park, panels (**e1–e7**) show Yulongwan Park, and panels (**f1–f7**) show Baisheng Park. For each compound, panel **1** shows the monthly mean VIIRS/DNB NTL radiance aggregated within the compound boundary (nW·cm^{-2}·sr^{-1}), and panels **2–7** show spatial snapshots at selected timestamps: 2017-01, 2023-05, 2024-01, 2024-08, 2025-01, and 2025-03. The figure is intended for visual interpretation; all eight compounds were included in the quantitative analyses.

2.2.2. Impervious Surface and Land Use

To further reveal internal structural differences and development levels of the parks, this study incorporates Sentinel-1 synthetic aperture radar (SAR) data and Sentinel-2 multispectral optical imagery to construct a multi-source remote sensing integration pathway. Considering the impact of regional cloud and fog conditions, single-scene high-quality images acquired between March and October each year were selected as the basis for annual analysis. A Random Forest supervised classification algorithm was then employed to distinguish major land cover types—including impervious surfaces, vegetation, water bodies, and bare land—and to extract annual impervious surface areas and land-cover evolution trends, thereby providing quantitative evidence for the spatial expansion and land-use characteristics of fraud compounds. Training samples were manually selected

based on high-resolution Google Earth imagery and Sentinel-1/2 visual interpretation, representing four land-cover classes: impervious surfaces, vegetation, water bodies, and bare land. The Random Forest classifier was evaluated using independent validation samples, with overall accuracy, the Kappa coefficient, user's accuracy, and producer's accuracy used as accuracy metrics. The available annual accuracy assessment results are reported in Appendix A, Table A1. These results are interpreted as internal validation diagnostics rather than independent field-based ground-truth verification, because sample selection and spatial autocorrelation may influence accuracy estimates.

2.2.3. Social Media Search Intensity

To measure Chinese-language online public attention related to cross-border telecommunications fraud, this study collected Baidu Index data using the keyword "telecom fraud" from January 2017 to March 2025, and aggregated daily or weekly frequencies into monthly series. This dataset was used to characterize the intensity and temporal dynamics of Chinese-language online search interest related to telecommunications fraud. As a representative indicator of Chinese-language internet search behavior, the Baidu Index can reflect temporal fluctuations in public attention to major social issues. Because many public reports, victims, and policy discussions related to cross-border telecommunications fraud are closely connected with Mainland China, search intensity recorded within China provides a useful proxy for the external information visibility of these issues. However, the Baidu Index should be interpreted as a complementary social sensing indicator rather than direct evidence of fraud activity within specific parks.

2.2.4. Auxiliary Data

The boundary data used in this study comprise two components: Myanmar's administrative boundaries obtained from the Humanitarian Data Exchange (HDX), and park boundaries manually delineated on Google Maps and calibrated using high-resolution imagery. All boundaries were projected to the WGS84 coordinate system (EPSG:4326) to ensure spatial analysis consistency.

2.2.5. Data Consistency Processing

Park boundaries were used as the unified statistical unit and spatial reference, with consistency constraints applied across data types. Missing nighttime-light data were interpolated and smoothed under controlled parameters to maintain temporal continuity and integrity. Optical and radar imagery retained their native resolution and spectral properties, with aggregated statistics aligned temporally (annual or monthly) to the NTL data. Social media data were aggregated from daily to monthly Baidu Index series and temporally aligned with other datasets.

In summary, a multi-source dataset encompassing "physical expansion–nighttime activity intensity–online public attention" was established, forming the data foundation for subsequent "space–time–representation" coupling analysis, as shown in Table 2.

Table 2. Multi-source indicator system for dynamic analysis of fraud parks.

Data Name	Source	Year	Spatial Resolution	Temporal Resolution	Acquisition Method
Nighttime Light Data	VIIRS-DNB	2017.01–2025.03	500m	Monthly	Google Earth Engine
Land Use Data	Sentinel-1 SAR, sentinel-2	2017.01–2025.03	10–30m	Annual	Google Earth Engine
Social Media Data	Baidu Index	2017.01–2025.03	——	Monthly	https://index.baidu.com, accessed on 25 May 2025
Boundary Data				Vector (HDX)	

2.3. Methodology

To address the scientific question of "space–time–representation" coupling, this study constructs a replicable multi-source fusion framework integrating remote sensing and social sensing data, as seen in Figure 4. The following sections elaborate the technical workflow and key algorithms in a hierarchical manner, following the logic of data acquisition, preprocessing, spatiotemporal analysis, and coupling analysis.

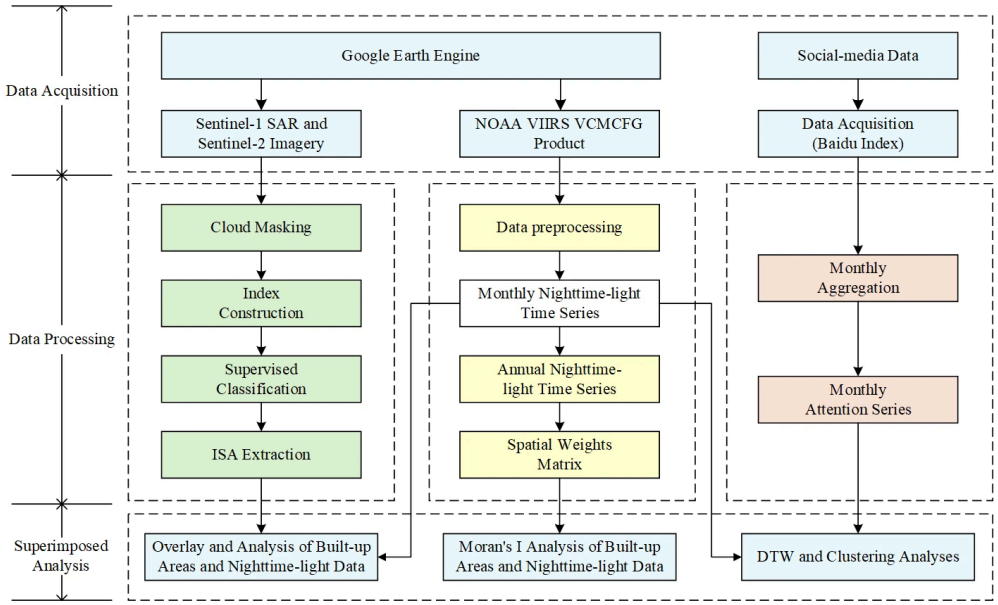


Figure 4. Framework of technical route and analytical process.

2.3.1. Remote Sensing Data Extraction on the GEE Platform

Based on manually delineated park boundaries (Shapefile), monthly VIIRS/DNB nighttime light imagery from 2017 to 2025 was retrieved using the Google Earth Engine (GEE) platform. The park boundaries were used as the region of interest (ROI) for spatial clipping, after which monthly mean nighttime light intensity values were calculated for each park, generating a complete time-series dataset covering park identifiers, temporal intervals, and brightness indicators.

To identify construction progress and spatial development intensity within the parks, contemporaneous Sentinel-1 and Sentinel-2 imagery was further extracted. Using a Random Forest classification algorithm, land cover was divided into four categories—impervious surfaces, water bodies, vegetation, and bare land. The model was trained with high-confidence samples to extract annual mean impervious surface areas (in km^2) and construct built-up area expansion sequences, providing quantitative foundations for analyzing park spatial growth and construction dynamics.

2.3.2. Nighttime Light Data Preprocessing

Considering that the original nighttime light (NTL) data are affected by factors such as cloud cover, observation discontinuities, gas-flare interference, and sensor drift, which can lead to missing and extreme values [28], this study established a preprocessing procedure to improve temporal continuity and reduce isolated abnormal fluctuations.

First, missing values were filled using linear interpolation based on adjacent valid observations. For single-month gaps, the missing value was estimated as the average of the preceding and subsequent valid observations [29]:

$$R_i^{(t)} = \frac{R_i^{(t-1)} + R_i^{(t+1)}}{2} \quad (1)$$

The variables are defined as follows:

Where $R_i^{(t)}$ represents the nighttime light intensity of park i in month t (unit: nW·cm^{-2}·sr^{-1}）; t denotes time (in months); i denotes the park identifier or name; $R_i^{(t-1)}$, $R_i^{(t+1)}$ represent the observed values of the preceding and subsequent months, respectively.

For consecutive missing values, linear interpolation was conducted between the nearest valid observations before and after the gap. Second, extreme outliers were detected using the Z-score method, with $|Z| > 2.5$ defined as the threshold for abnormal observations [30]. These isolated abnormal values were adjusted using interpolation between adjacent valid observations. Third, a three-month moving average filter was applied to reduce short-term fluctuations and improve the readability of temporal trends [26].

In total, the original monthly NTL dataset contained 792 compound-month observations. Among them, 102 missing observations (12.88%) were interpolated, and 14 extreme observations (1.77%) were identified using the $|Z| > 2.5$ criterion and were adjusted through interpolation. The preprocessing summary by compound is reported in Appendix A, Table A2. Because the proportion of extreme-value adjustment was small, preprocessing was mainly used to improve temporal continuity and reduce isolated spikes rather than to reshape long-term trends.

Finally, to mitigate the short-term fluctuations, a symmetric moving average filter with a window width k = 3 was applied:

$$\overline{R_i^{(t)}} = \frac{1}{k} \sum_{j=t-\left|\frac{k}{2}\right|}^{t+\left|\frac{k}{2}\right|} R_i^{(j)} \quad (2)$$

where $\overline{R_i^{(t)}}$ denotes the smoothed nighttime light intensity of park i in month t, $R_i^{(j)}$ denotes the interpolated or adjusted NTL value in month j, and $k = 3$ denotes the moving-average window width.

2.3.3. Spatial Autocorrelation and Built-Up Area Coupling Methods

To examine local brightness clustering around the selected compounds, a spatial autocorrelation analysis was conducted using nighttime light values within each compound boundary and its surrounding buffer area. For each compound, a 5 km buffer was generated around the manually delineated boundary to capture the surrounding nighttime-light environment, including nearby settlements, roads, and possible overglow from adjacent light sources. The spatial units for the autocorrelation analysis were VIIRS/DNB nighttime-light pixels within the compound boundary and the 5 km buffer.

A spatial weight matrix was constructed based on the spatial adjacency or distance relationships among NTL pixels in ArcGIS Pro 3.0.2. Global Moran's I was used to evaluate whether NTL values within the defined analysis units exhibited overall spatial clustering [31]. The Anselin Local Moran's I (LISA) method was then applied to identify local clusters and outliers, including high–high, high–low, low–high, and low–low patterns [32]. These results were used to describe local nighttime-light clustering patterns

rather than to infer the non-random spatial distribution of compound locations, operational networks, or spillover effects.

To further examine whether nighttime brightness was accompanied by physical construction, annual built-up area was compared with annual mean NTL radiance at the compound-year level [33]. Because repeated observations from the same compounds are not fully independent, and because the 2025 NTL data cover only January–March, the annual BUA–NTL relationship was interpreted as an exploratory association rather than causal evidence.

2.3.4. Nonlinear Alignment of Heterogeneous Time Series: Dynamic Time Warping (DTW)

Since nighttime light (NTL) remote-sensing data are primarily produced as monthly composites and thus updated with a temporal lag, while online search intensity may fluctuate more rapidly in response to public events and media exposure, discrepancies arise in their response rates and fluctuation patterns. Such differences may lead to temporal misalignment or structural bias when the two datasets are directly compared. To address this, the study applies the Dynamic Time Warping (DTW) algorithm, which performs nonlinear temporal axis transformation to achieve optimal alignment between monthly sequences from different data sources [34,35].

Let $X = \{x_1, x_2, \ldots, x_n\}$ denote the nighttime light intensity series and $Y = \{y_1, y_2, \ldots, y_n\}$ denote the social media attention series. A distance matrix $D(i,j) = (x_i - y_j)^2$ is constructed, and under the constraints of continuity, monotonicity, and boundary conditions, the minimal cumulative cost path W is identified. The minimum cumulative distance $DTW(X,Y) = min\sum_{k=1}^{K} D_{(\omega_k)}$ is then computed to quantitatively represent the dynamic matching degree between the two data series. During the matching process, Euclidean distance was used as the metric with a global path strategy to identify synchronization, lag, and asynchrony between brightness variation and public attention responses, thereby avoiding misjudgments arising from inconsistent temporal granularity [36].

2.3.5. Exploratory Compound Grouping Based on DTW Distance

After characterizing the temporal alignment between nighttime light intensity and online public attention, this study further examined similarities in nighttime light evolution among the eight compounds. Pairwise DTW distances were calculated between the NTL trajectories of each compound, producing an 8×8 dissimilarity matrix that represents temporal differences among compounds. Because standard K-means is designed for Euclidean feature spaces rather than precomputed distance matrices, the DTW-based grouping is interpreted as an exploratory typology rather than a formal predictive classification. To assess the robustness of the grouping, hierarchical clustering based on the same pairwise DTW dissimilarity matrix was also conducted as a sensitivity check. The number of groups was evaluated using silhouette values for alternative cluster numbers.

3. Results

This chapter draws on multi-source datasets from 2017 to 2025 to examine the three-dimensional relationship among physical expansion (BUA), activity intensity (NTL), and informational visibility (Baidu Index). It sequentially presents the coupling between compound expansion and nighttime brightness, the structure of spatial clustering, differences in public discourse–nighttime light alignment, and temporal dislocations under the impact of governance interventions.

3.1. Temporal Coupling Between Physical Expansion and Nighttime Activity Intensity

The built-up areas of the representative compounds exhibit an overall upward trend, although the pace and magnitude of expansion vary substantially across sites (Figure 5). Among them, Huanya, KK Park, and Yatai City show the most pronounced expansion, increasing from 0.001 km^2 to 0.227 km^2, from 0.071 km^2 to 1.033 km^2, and from 0.121 km^2 to 0.628 km^2, respectively (+28,325%, +1354.51%, and +420.32%). Dingsheng Compound and Yulongwan Compound display moderate expansion, increasing from 0.005 km^2 to 0.021 km^2 and from 0.173 km^2 to 0.395 km^2, respectively (+324% and +128.65%). By contrast, the increases observed in Daxiang Compound and Baisheng are relatively limited, rising from 0.019 km^2 to 0.039 km^2 and from 0.018 km^2 to 0.028 km^2, respectively. Jinxin Compound, however, shows a decline by the end of the study period, decreasing from 0.171 km^2 to 0.123 km^2 (−28.36%).

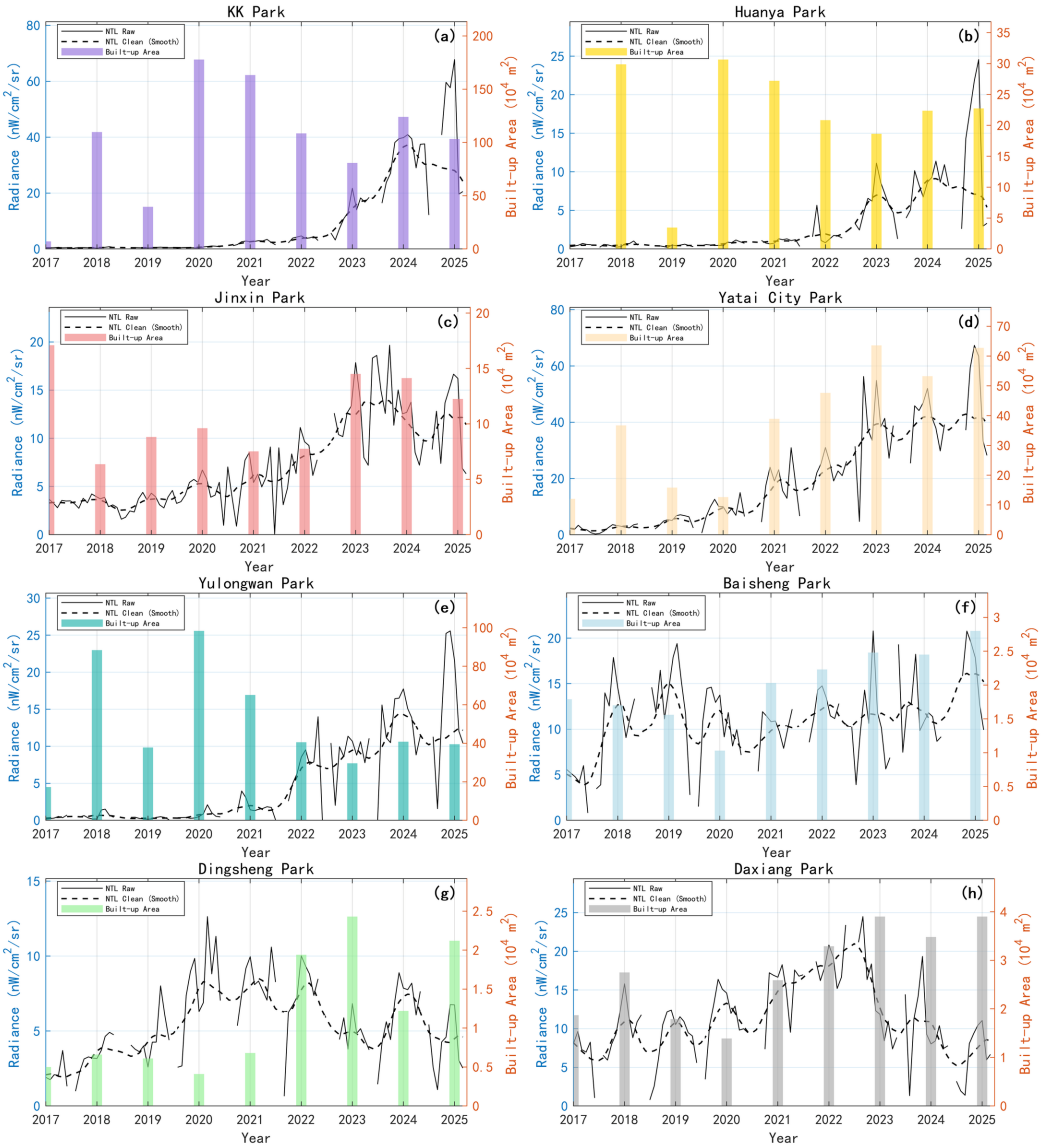


Figure 5. Temporal Dynamics of Built-up Area and Nighttime Light Intensity (NTL) in eight selected compounds. (**a**) KK Park; (**b**) Huanya Park; (**c**) Jinxin Park; (**d**) Yatai City Park; (**e**) Yulongwan Park; (**f**) Baisheng Park; (**g**) Dingsheng Park; (**h**) Daxiang Park. The annual BUA–NTL correlation analysis was conducted using complete years from 2017 to 2024, while 2025 NTL observations were treated as partial-year data and used only for temporal interpretation.

Because the 2025 NTL record extends only to March 2025, 2025 was treated as a partial-year observation and excluded from the annual BUA–NTL correlation analysis. The annual correlation analysis was therefore recalculated using complete years from 2017 to 2024 (N = 64). At the park–year level, the association between BUA and annual mean NTL was weak and statistically insignificant (Pearson's r = 0.091, $p = 0.475$; Spearman's $\rho = -0.102$, $p = 0.420$). To account for repeated observations from the same compounds, a sensitivity analysis using within-compound demeaned variables was also conducted. The within-compound association remained weak and statistically insignificant (Pearson's r = 0.201, $p = 0.110$; Spearman's $\rho = 0.178$, $p = 0.159$). These results suggest that built-up expansion and nighttime brightness are not uniformly coupled across compounds and years. Therefore, the BUA–NTL relationship is interpreted as an exploratory association rather than causal evidence. Accordingly, the observed BUA–NTL patterns are used as directional evidence for interpreting potential coupling and decoupling between physical expansion and nighttime radiance, rather than as precise statistical estimates. further comparison across key stages reveals that brightness and area do not always evolve synchronously:

(1) Anomalous increases in brightness with limited changes in area: In 2020 Q1, NTL in Huanya and Daxiang increased sharply by 48% and 37%, respectively, while BUA changed by less than 5% over the same period. This pattern may correspond to energy-intensive activities, enhanced external lighting, or a sudden rise in nighttime radiance rather than simultaneous construction expansion.

(2) Marginal area growth accompanied by a substantial decline in brightness: In 2023 Q3, BUA in KK Park increased slightly by 8%, whereas NTL dropped sharply by 32%. This suggests a "brightness–area" decoupling pattern, in which physical expansion and nighttime radiance did not change synchronously. The observed decline in brightness may be associated with multiple possible factors, such as reduced electricity use, temporary lighting changes, changes in surrounding light sources, or sensor- and environment-related effects. These explanations cannot be distinguished using NTL and BUA data alone.

3.2. Spatial Autocorrelation and Built-Up Area Coupling Analysis

The results of global spatial autocorrelation indicate that NTL in the study area exhibits significant clustering (Moran's I = 0.2476, Z = 4.84, $p < 0.0001$), suggesting that NTL values within the defined compound–buffer analysis units exhibit local spatial clustering. This result should not be interpreted as evidence that compound locations themselves are non-randomly distributed or that operational spillover exists between compounds.

The LISA results further show the coexistence of local high-brightness clusters and high-brightness outliers. The Dingsheng–KK Park area and its 5 km buffer zone identified a typical High–High (HH) cluster, indicating that high NTL values were surrounded by similarly high values within the local analysis window. By contrast, Huanya and Daxiang appear as High–Low (HL) outliers within a low-density background, indicating locally elevated nighttime brightness relative to the surrounding low-brightness background.

To examine whether brightness clustering necessarily corresponds to physical expansion, a further bivariate Moran's I analysis was conducted. The results show that the global coupling between NTL and BUA is not statistically significant ($I = -0.033$, $p = 0.42$). This indicates that, at the spatial level, "high brightness" is not necessarily accompanied by greater impervious surface expansion. At the local level, Daxiang Compound represents a typical HL outlier, characterized by high brightness but low impervious surface area. This pattern suggests brightness–BUA decoupling, but it does not by itself identify the underlying cause of elevated nighttime radiance.

3.3. DTW Alignment Between Nighttime Lights and Online Public Attention

After Z-score standardization of NTL and Baidu Index values, DTW distance was used to measure the degree of nonlinear alignment between the two monthly time series (Figure 6). Since DTW is a similarity-based metric rather than a hypothesis test, alignment levels were classified according to the empirical distribution of all DTW distances. Values below the 25th percentile were interpreted as relatively strong NTL–public attention correspondence, whereas values above the 75th percentile were interpreted as relatively weak NTL–public attention correspondence.

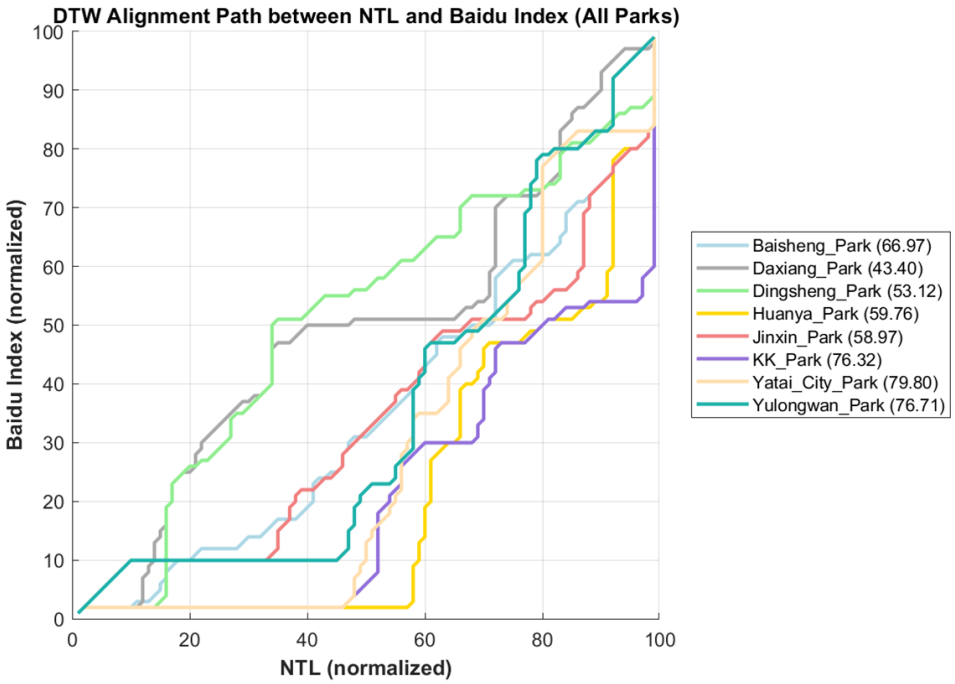


Figure 6. DTW Alignment Paths between Normalized Nighttime Light Intensity (NTL) and Baidu Search Index for All Parks.

The results reveal substantial differentiation across compounds. Daxiang Compound records the smallest DTW distance (43.40), indicating a high degree of consistency between online attention and nighttime light variation. Dingsheng and Huanya follow, with distances of 53.12 and 59.76, respectively. Jinxin and Baisheng fall within the intermediate range, with DTW distances of 58.97 and 66.97, suggesting weaker coupling than the preceding compounds. By contrast, KK Park, Yulongwan, and Yatai City all have DTW distances greater than 76, indicating weaker temporal correspondence between nighttime brightness changes and online search interest.

These differences suggest that the relationship between observed nighttime activity intensity and external information visibility varies substantially across compounds. However, weaker NTL–public attention correspondence should not be interpreted as evidence of compound-specific information isolation or lower activity intensity, because the Baidu Index reflects general Chinese-language online search interest rather than direct operational conditions within individual compounds.

3.4. Exploratory Compound Typology Based on DTW Dissimilarity

Based on the 8 × 8 DTW dissimilarity matrix derived from nighttime light trajectories, exploratory grouping was used to characterize similarities in NTL evolution among the eight compounds (Figure 7). Because the sample size is small and the input is a DTW-derived dissimilarity matrix rather than a conventional Euclidean feature matrix,

the grouping results are interpreted as a descriptive typology rather than a formal classification. As a robustness check, hierarchical clustering based on the same DTW dissimilarity matrix was conducted. The silhouette values for alternative group numbers were 0.326 for k = 2, 0.461 for k = 3, and 0.383 for k = 4, supporting the use of a three-group exploratory typology. The grouping results were further interpreted together with the NTL–Baidu Index DTW alignment results to characterize differences in NTL–public attention correspondence:

(1) Strong public-attention correspondence type (Daxiang and Dingsheng): Daxiang and Dingsheng exhibited relatively similar nighttime light evolution trajectories. Combined with the NTL–Baidu Index alignment results, these compounds showed relatively strong correspondence between nighttime light changes and online public attention.

(2) Moderate public-attention correspondence type (Huanya, Jinxin, and Baisheng): The cluster containing these compounds showed intermediate similarity in nighttime light evolution. Combined with the NTL–Baidu Index alignment results, they exhibited moderate correspondence between observed activity changes and online attention, with stage-specific temporal mismatches.

(3) Weak public-attention correspondence type (KK Park, Yulongwan, and Yatai City): The cluster containing these compounds showed distinct nighttime light evolution patterns. Combined with the NTL–Baidu Index alignment results, these compounds exhibited weaker correspondence between nighttime light changes and online public attention. This pattern reflects relatively low visibility in the Baidu Index series, but it should not be interpreted as direct evidence of compound-specific operational conditions.

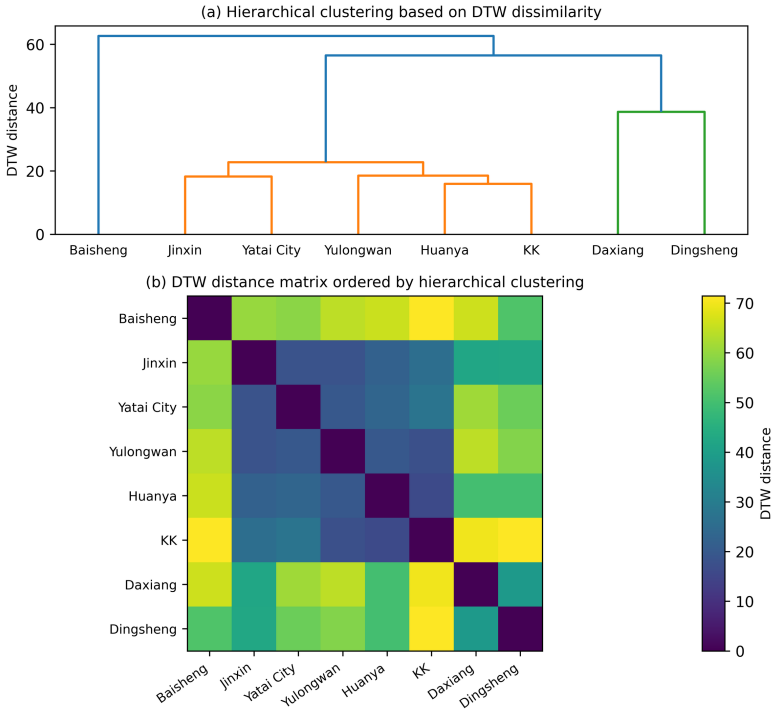


Figure 7. DTW-derived dissimilarity structure and exploratory grouping of the eight selected compounds. (**a**) Hierarchical clustering based on the pairwise DTW dissimilarity matrix of nighttime-light trajectories. Different branch colors in panel (**a**) indicate clusters separated by the hierarchical clustering algorithm. (**b**) DTW distance matrix reordered according to the hierarchical clustering result. The grouping is used as an exploratory typology of nighttime-light evolution patterns rather than as a formal predictive classification.

This exploratory typology provides a descriptive basis for differentiated monitoring and further investigation. Compounds with stronger NTL-public attention correspondence may be more readily reflected in open-source information and public search dynamics, whereas compounds with weaker correspondence may benefit from additional remote-sensing comparison, field verification where feasible, and cross-border information sharing. However, the typology should be interpreted as a monitoring and prioritization tool rather than as direct evidence of compound-specific operational status.

3.5. Event-Related Temporal Comparison Between Nighttime Lights and Online Public Attention

By comparing the indexed NTL and composite online public attention series at selected event-related observation periods (Figure 8), the results suggests that nighttime-light dynamics and online public attention did not change synchronously. Around the disclosure-related observation periods in September and November 2023, NTL had already shown a sustained downward tendency across representative compounds, with an average decline of approximately 8–10%. Between May and August 2024, NTL remained at a relatively low level, a temporal pattern that overlapped with publicly reported cross-border enforcement-related activities during this period. In early 2025, light intensity continued to decrease, coinciding with publicly reported announcements concerning arrests and transfers of individuals in Wa state, Dangyang and Mengxiu. These temporal patterns suggest that nighttime lights may provide a complementary indicator of changes in surface-level activity intensity, whereas online public attention captures external information visibility and public search responses.

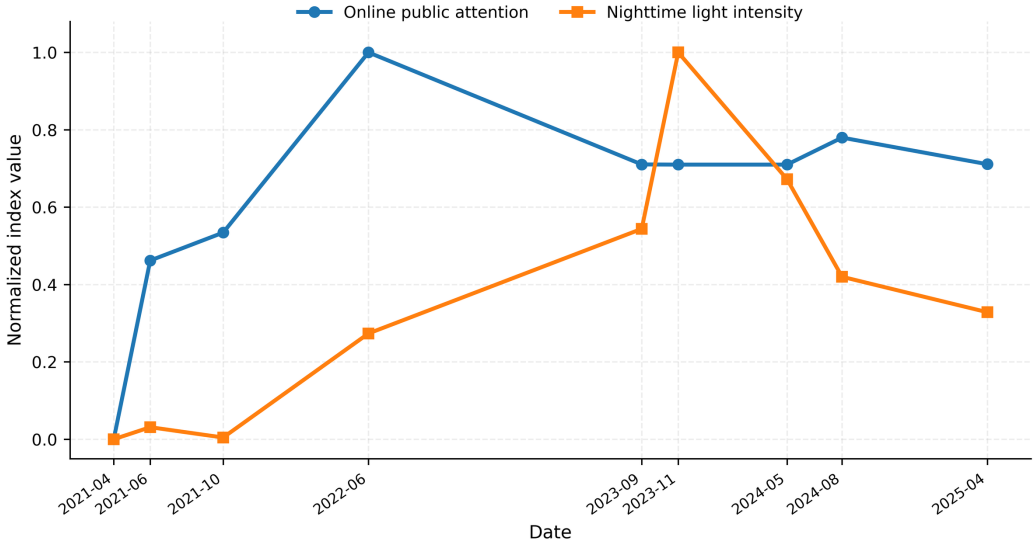


Figure 8. Indexed comparison of online public attention and nighttime-light intensity at selected event-related observation periods. Both series were normalized using min–max scaling to compare their relative temporal changes on a common scale.

In summary, the results show that the "physical expansion–nighttime activity–informational visibility" relationship of fraud compounds does not follow a linear pattern of synchronous co-movement. Instead, partial coupling and stage-specific decoupling van be observed between spatial activity indicators and public attention during selected event-related periods. Moreover, informational visibility varies across compounds in a stratified manner, suggesting the potential value of differentiated monitoring and prioritization.

4. Discussion and Conclusions

This study uses nighttime lights (NTL), impervious surface/built-up area expansion (BUA), and social media search intensity (Baidu Index) as three complementary proxy indicators to construct an integrated "space–time–representation" framework for characterizing the dynamic evolution of fraud compounds in northern Myanmar under conditions of limited field data. This section discusses the findings in terms of coupling and decoupling mechanisms, differences in informational visibility, governance implications, limitations, and transferability.

4.1. Physical Expansion and Activity Intensity

Overall, the revised BUA–NTL comparison suggests that built-up expansion and nighttime brightness are not uniformly coupled across compounds and years. Nighttime lights can therefore serve as an indirect proxy for nighttime radiance and activity intensity, complementing built-up area indicators of physical development. However, the two types of deviation observed in the results have clear mechanistic implications. First, "a sharp increase in brightness with limited area change" may reflect energy-intensive activity, enhanced external lighting, or short-term concentrated radiance changes rather than synchronous construction expansion. Second, "a slight increase in area accompanied by a sharp decline in brightness" may be associated with temporary lighting changes, reduced electricity use, operational adjustment, changes in surrounding light sources, or sensor- and environment-related effects. In other words, NTL is more sensitive to nighttime radiance and electricity-use-related activity, whereas BUA is more sensitive to physical construction and spatial capacity. Combining the two makes it possible to distinguish between situations in which a compound is "more extensively built but not necessarily brighter" and those in which it is "brighter but not necessarily more extensively built," thereby reducing the risk of misinterpretation when relying on a single remote-sensing indicator in grey-space contexts.

4.2. Spatial Structure

The global Moran's I indicates that NTL values within the defined compound–buffer analysis units exhibit significant spatial clustering. This result should be interpreted as evidence of spatial clustering in nighttime brightness within the analyzed local light environments, rather than as evidence that compound locations themselves are non-randomly distributed. The HH clusters and HL outliers identified by LISA suggest two distinct local nighttime-light patterns. The former indicates that high NTL values are surrounded by similarly high values within the local analysis window. The latter refers to locally elevated nighttime brightness relative to a lower-brightness surrounding background, which may be associated with localized lighting, temporary radiance changes, nearby infrastructure, or other local factors. This distinction indicates that "whether a site is bright" alone is insufficient for assessing its interpretation; spatial context and neighborhood structure are also important.

4.3. Differences in Informational Visibility

The three patterns revealed by DTW alignment and exploratory grouping characterize differences in the correspondence between nighttime-light dynamics and online public attention. The strong public-attention correspondence type indicates that NTL changes and Baidu Index fluctuations show relatively similar temporal behavior. The moderate public-attention correspondence type reflects stage-specific temporal mismatch between observed nighttime-light changes and online public attention. The weak public-attention correspondence type indicates that NTL changes and Baidu Index fluctuations

are less closely aligned. Rather, weak correspondence may be related to keyword selection, platform coverage, media exposure, information availability, Chinese-language search behavior, and uneven online participation patterns. Therefore, compounds with weak NTL–public attention correspondence may require further verification through remote sensing and multi-source open-source evidence, and low public attention should not be interpreted as evidence of low nighttime activity intensity.

4.4. Governance Implications

From an applied perspective, the exploratory typology can support differentiated monitoring and prioritization under data-scarce conditions. Compounds with stronger NTL–public attention correspondence may be more readily reflected in open-source information and public search dynamics. Compounds with moderate correspondence require continued comparison between nighttime-light dynamics and public attention to avoid relying on a single indicator. Compounds with weaker NTL–public attention correspondence may benefit from additional remote-sensing comparison, field verification where feasible, and cross-border information sharing. More broadly, the event-related comparison suggests that nighttime-light dynamics and online public attention do not necessarily evolve synchronously around selected publicly reported events. Nighttime lights may capture changes in surface-level nighttime radiance and electricity-use-related activity, whereas public attention reflects external information visibility and public search responses after relevant information enters the public domain. Their complementarity helps distinguish changes in observed nighttime radiance from changes in public attention.

From this perspective, the proposed remote sensing and social sensing framework can help make concealed forms of digital socio-spatial harm more visible. For scholars, it provides a transferable framework for examining spatially hidden illicit economies under data-scarce conditions. For policy makers and community leaders, it can support evidence informed prioritization for further investigation, labor protection, humanitarian response, and cross-border governance coordination. However, such monitoring should not be treated as direct proof of illicit activity but as a screening and prioritization tool that requires follow-up verification.

4.5. Limitations, Transferability, and Future Work

This study has several limitations. First, NTL cannot distinguish among different types of activity and may be affected by temporary light sources, gas flaring, changes in electricity supply or lighting practices, and sensor noise. Second, BUA or built-up area estimates are influenced by clouds, seasonality, and classification errors, which may produce fluctuations in individual years or months that do not have a physical interpretation. Third, the Baidu Index reflects external attention within the Chinese-language internet environment and is therefore subject to platform specificity and visibility bias; it cannot capture non-Chinese information spheres or communication occurring outside public search behavior. Given the small number of selected compounds, the coarse spatial resolution of VIIRS nighttime-light data, and the lack of field-based verification, the statistical results should be interpreted as directional and exploratory evidence rather than robust causal or predictive evidence. Future research could introduce higher-resolution nighttime light data or high-resolution optical imagery to verify key periods, incorporate additional social sensing channels across multiple platforms and languages, and improve inferential reliability through robustness checks, such as threshold sensitivity analysis and event-window comparisons. Compared with conventional crime mapping and prediction studies that often depend on detailed incident records and dense urban sensing data, the proposed framework is designed for data-scarce and field-inaccessible environments where direct

observations are limited. Future research may explore whether advanced spatiotemporal prediction models can be integrated when more consistent observational data and larger samples of known compounds become available.

This framework can be transferred to other data-scarce or field-inaccessible regions. VIIRS nighttime lights and global built-up area products can provide consistent proxies for activity and expansion, while DTW, spatial autocorrelation, and exploratory grouping methods can be adapted or reused. For different regional contexts, only the social sensing indicators need to be adapted to the local information ecology, such as Google Trends, X/Twitter, or the visibility of public Telegram channels. However, under conditions of high cloud cover, highly reflective land surfaces, wartime electricity control, or strong information regulation, multi-source corroboration and explicit uncertainty reporting should be emphasized to avoid mistaking changes in visibility for changes in activity.

Author Contributions: Conceptualization, Xiaofang Zhai and Zhifeng Xiao; methodology, Fan Zhang; formal analysis, Fan Zhang; data curation, Fan Zhang; software, Haoyang Xu; validation, Haoyang Xu and Weiqi Yan; visualization, Haoyang Xu; writing—original draft preparation, Fan Zhang and Xiaofang Zhai; writing—review and editing, Zhifeng Xiao; supervision, Weiqi Yan and Zhifeng Xiao; project administration, Xiaofang Zhai. All authors have read and agreed to the published version of the manuscript.

Funding: This work wassupported by the National Key Research and Development Program of Chinaunder Grant 2024YFC3015503.

Data Availability Statement: The processed datasets and analysis scripts are openly available at [https://doi.org/10.5281/zenodo.22879926]. Due to licensing restrictions, the original VIIRS, Sentinel-1/2, and Baidu Index datasets were obtained from their respective providers and cannot be redistributed.

Acknowledgments: The authors acknowledge the Supercomputing Center of Wuhan University for providing computational resources and computational support. The authors also thank anonymous reviewers for their constructive comments.

Conflicts of Interest: The authors declare no conflicts of interest.

Appendix A

Appendix A.1. Random Forest Classification Accuracy Assessment

Table A1. Available Random Forest classification accuracy assessment results.

Year	Overall Accuracy	Kappa Coefficient
2018	0.9812	0.9748
2019	0.9788	0.9716
2020	0.9844	0.9751
2021	0.9736	0.9648
2023	0.9809	0.9744
2024	0.9962	0.9949
2025	0.9575	0.9429

Note: The accuracy metrics were exported from Google Earth Engine classification outputs. User's accuracy and producer's accuracy were generated in the GEE validation outputs where available, but complete annual confusion matrices and class-level accuracy tables were not retained for all years. Therefore, these results are reported as internal validation diagnostics rather than independent field-based ground-truth verification. Therefore, the classification results are used to support relative built-up area extraction and spatiotemporal comparison rather than exact land-cover mapping.

Appendix A.2. Nighttime Light Preprocessing Summary

Table A2. Summary of missing and extreme NTL observations.

Compound	Total Observations	Missing Interpolated	Extreme Adjusted |Z| > 2.5	Valid After Preprocessing
Daxiang	99	12	1	99
Huanya	99	15	3	99
Yulongwan	99	14	3	99
Yatai City	99	16	2	99
Baisheng	99	17	0	99
Dingsheng	99	13	1	99
KK Park	99	12	3	99
Jinxin	99	3	1	99
Total	792	102	14	792

Note: Missing observations were filled using interpolation based on adjacent valid values. Extreme observations were identified using the $|Z| > 2.5$ criterion within each compound-level monthly NTL series and adjusted through interpolation. The adjusted extreme observations accounted for 1.77% of all compound-month observations.

References

1. Loggen, J.; Moneva, A.; Leukfeldt, E. A systematic narrative review of pathways into, desistance from, and risk factors of financial-economic cyber-enabled crime. *Comput. Law Secur. Rev.* **2024**, *52*, 105858. [CrossRef]
2. Hu, Z.; Konrad, V. Repositioning security spaces of exclusion, exception, and integration in China–Southeast Asia borderlands. *Reg. Cohes.* **2021**, *11*, 1–25. [CrossRef]
3. Corn, G.P. Cyber National Security: Navigating Gray-Zone Challenges in and through Cyberspace. In *Complex Battlespaces: The Law of Armed Conflict and the Dynamics of Modern Warfare*; Williams, W.S., Ford, C.M., Eds.; Oxford University Press: New York, NY, USA, 2019; pp. 345–428. [CrossRef]
4. Davies, T. 'Sacrifice zone': The environment–territory–place of disposable lives. *Community Dev. J.* **2021**, *56*, 220–243. [CrossRef]
5. Balsas, C.J.L. Where does technology fit in the geospatial design and planning professions? In *Multi Conference on Computer Science and Information Systems, MCCSIS 2019—Proceedings of the International Conferences on ICT, Society and Human Beings 2019, Connected Smart Cities 2019 and Web Based Communities and Social Media 2019*; IADIS Press: Porto, Portugal, 2019; pp. 257–266. [CrossRef]
6. Li, X.; Liu, S.; Jendryke, M.; Li, D.; Wu, C. Night-time light dynamics during the Iraqi Civil War. *Remote Sens.* **2018**, *10*, 858. [CrossRef]
7. Feng, Y.; Liu, S.; Tang, L. Automatic extraction and change monitoring of fire disaster events based on high-resolution nighttime light remote sensing images. *Proc. SPIE* **2020**, *11533*, 115330A. [CrossRef]
8. Noor, A.M.; Alegana, V.A.; Gething, P.W.; Tatem, A.J.; Snow, R.W. Using remotely sensed night-time light as a proxy for poverty in Africa. *Popul. Health Metr.* **2008**, *6*, 5. [CrossRef] [PubMed]
9. Dong, B.; Zhang, R.; Li, S.; Ye, Y.; Huang, C. A meta-analysis for the nighttime light remote sensing data applied in urban research. *Sci. Remote Sens.* **2024**, *6*, 100186. [CrossRef]
10. Tan, X.; Zhu, X.; Chen, J.; Chen, R. Modeling the direction and magnitude of angular effects in nighttime light remote sensing. *Remote Sens. Environ.* **2022**, *273*, 112834. [CrossRef]
11. Zheng, Q.; Seto, K.C.; Zhou, Y.; You, S.; Weng, Q. Nighttime light remote sensing for urban applications: Progress, challenges, and prospects. *ISPRS J. Photogramm. Remote Sens.* **2023**, *198*, 156–174. [CrossRef]
12. Vaidyanathan, U.; Sun, Y.; Shekel, T.; Chou, K.; Galea, S.; Gabrilovich, E.; Wellenius, G.A. An evaluation of Internet searches as a marker of trends in population mental health in the US. *Sci. Rep.* **2022**, *12*, 8946. [CrossRef] [PubMed]
13. Fariello, G.; Jemielniak, D. The changing language and sentiment of conversations about climate change in Reddit posts over sixteen years. *Commun. Earth Environ.* **2025**, *6*, 3. [CrossRef]
14. Lim, C.; Kim, S. Examining factors influencing the user's loyalty on algorithmic news recommendation service. *Humanit. Soc. Sci. Commun.* **2024**, *11*, 10. [CrossRef]
15. Zhou, S.; Yang, X.; Wang, Y.; Zheng, X.; Zhang, Z. Affective agenda dynamics on social media: Interactions of emotional content posted by the public, government, and media during the COVID-19 pandemic. *Humanit. Soc. Sci. Commun.* **2023**, *10*, 797. [CrossRef]
16. Lekkas, D.; Jacobson, N.C. Breaking the silence: Leveraging social interaction data to identify high-risk suicide users online using network analysis and machine learning. *Sci. Rep.* **2024**, *14*, 19395. [CrossRef] [PubMed]

17. Zhou, Z.; Elejalde, E. Unveiling the silent majority: Stance detection and characterization of passive users on social media using collaborative filtering and graph convolutional networks. *EPJ Data Sci.* **2024**, *13*, 28. [CrossRef]
18. Zhao, N.; Cao, G.; Zhang, W.; Samson, E.L.; Chen, Y. Remote sensing and social sensing for socioeconomic systems: A comparison study between nighttime lights and location-based social media at the 500 m spatial resolution. *Int. J. Appl. Earth Obs. Geoinf.* **2020**, *87*, 102058. [CrossRef]
19. Qi, L.; Li, J.; Wang, Y.; Gao, X. Urban observation: Integration of remote sensing and social media data. *IEEE J. Sel. Top. Appl. Earth Obs. Remote Sens.* **2019**, *12*, 4252–4264. [CrossRef]
20. Bennett, M.; Smith, L. Advances in using multitemporal night-time lights satellite imagery to detect, estimate, and monitor socioeconomic dynamics. *Remote Sens. Environ.* **2017**, *192*, 176–197. [CrossRef]
21. Marwen, B.; Mohamed, F.; Riadh, F.I. Suspicious local event detection in social media and remote sensing: Towards a geosocial dataset construction. In *Proceedings of the 2020 5th International Conference on Advanced Technologies for Signal and Image Processing (ATSIP), Sousse, Tunisia, 2–5 September 2020*; IEEE: Piscataway, NJ, USA, 2020; pp. 1–6. [CrossRef]
22. Liang, X.; Zhou, L.; Wang, S.; Zhao, X.; Xue, J.; Ding, Q.; Pan, Y. Spatiotemporal crime prediction and fairness-constrained spatial optimization with deep reinforcement learning for patrol region design. *Int. J. Appl. Earth Obs. Geoinf.* **2025**, *145*, 104973. [CrossRef]
23. He, Z.; Gu, Y.; Gong, Y.; Wu, L.; Zhou, M. Analyzing the joint influence of urban facilities and street perception characteristics on street robbery. *J. Geovisualization Spat. Anal.* **2025**, *9*, 22. [CrossRef]
24. Dong, Q.; Li, Y.; Zheng, Z.; Wang, X.; Li, G. ST3DNetCrime: Improved ST-3DNet model for crime prediction at fine spatial temporal scales. *ISPRS Int. J. Geo-Inf.* **2022**, *11*, 529. [CrossRef]
25. Peng, X. Playing with fire: How engagement with illicit economies shapes the survival and resilience of ethnic armed organisations in the China-Myanmar borderlands. *China Perspect.* **2024**, *138*, 9–20. [CrossRef]
26. Elvidge, C.; Baugh, K.; Zhizhin, M.; Hsu, F.; Ghosh, T. VIIRS night-time lights. *Int. J. Remote Sens.* **2017**, *38*, 5860–5879. [CrossRef]
27. Zhao, N.; Hsu, F.; Cao, G.; Samson, E. Improving accuracy of economic estimations with VIIRS DNB image products. *Int. J. Remote Sens.* **2017**, *38*, 5899–5918. [CrossRef]
28. Mills, S. VIIRS day-night band (DNB) electronic hysteresis: Characterization and correction. *Proc. SPIE* **2016**, *9972*, 99720K. [CrossRef]
29. Liu, Q.; Fan, J.; Zuo, J.; Li, P.; Shen, Y.; Ren, Z.; Zhang, Y. A spatiotemporally constrained interpolation method for missing pixel values in the Suomi-NPP VIIRS monthly composite images: Taking Shanghai as an example. *Remote Sens.* **2023**, *15*, 2480. [CrossRef]
30. Duc, C.; Hirakawa, T.; Fukui, H. Normalization of VIIRS DNB images for improved estimation of socioeconomic indicators. *Int. J. Digit. Earth* **2020**, *14*, 540–554. [CrossRef]
31. Eshetie, S.M. Exploring urban land surface temperature using spatial modelling techniques: A case study of Addis Ababa city, Ethiopia. *Sci. Rep.* **2024**, *14*, 6323. [CrossRef] [PubMed]
32. Hou, K.; Zhu, L. Spatial correlations between cultural ecosystem services and human activities along the Shenyang Hun River corridor. *Sci. Rep.* **2025**, *15*, 27781. [CrossRef] [PubMed]
33. Li, Y.; Shangguan, S.; Li, W.; Liu, S.; Li, Y.; Han, R.; Xu, J. Spatial–temporal distribution of farmland occupation and compensation and its impact on ecological service value in China from 1990 to 2021. *Sci. Rep.* **2025**, *15*, 98742. [CrossRef] [PubMed]
34. Mueen, A.; Keogh, E.J. Extracting optimal performance from dynamic time warping. In *Proceedings of the 22nd ACM SIGKDD International Conference on Knowledge Discovery and Data Mining*; Association for Computing Machinery: New York, NY, USA, 2016; pp. 2129–2130. [CrossRef]
35. Maus, V.; Câmara, G.; Cartaxo, R.; Sánchez, A.; Ramos, F.; Queiroz, G.R. A time-weighted dynamic time warping method for land-use and land-cover mapping. *IEEE J. Sel. Top. Appl. Earth Obs. Remote Sens.* **2016**, *9*, 3729–3739. [CrossRef]
36. Gwalani, H. Studying long-term user behaviour using dynamic time warping for customer retention. In *Proceedings of the Fifteenth ACM International Conference on Web Search and Data Mining*; Association for Computing Machinery: New York, NY, USA, 2022; pp. 625–628. [CrossRef]

Disclaimer/Publisher's Note: The statements, opinions and data contained in all publications are solely those of the individual author(s) and contributor(s) and not of MDPI and/or the editor(s). MDPI and/or the editor(s) disclaim responsibility for any injury to people or property resulting from any ideas, methods, instructions or products referred to in the content.